Journal of Dynamic Systems, Measurement, and Control. Received February 18, 2014;
Accepted manuscript posted October 13, 2014. doi:10.1115/1.4028787

A Closed-Form Solution for Selecting Maximum Critically Damped Actuator Impedance Parameters

Nicholas Paine
Graduate Research Assistant
Department of Electrical and Computer Engineering
University of Texas
Austin, Texas 78705
Email: npaine@utexas.edu

Luis Sentis
Assistant Professor
Department of Mechanical Engineering
University of Texas
Austin, Texas 78705
Email: lsentis@austin.utexas.edu

This paper introduces a simple and effective method for selecting the maximum feedback gains in PD-type controllers applied to actuators where feedback delay and derivative signal filtering are present. The method provides the maximum feedback parameters that satisfy a phase margin criteria, producing a closed-loop system with high stability and a dynamic response with near-minimum settling time. Our approach is unique in that it simultaneously possesses 1) a model of real-world performance-limiting factors (i.e. filtering and delay), 2) the ability to meet performance and stability criteria, and 3) the simplicity of a single closed-form expression. A central focus of our approach is the characterization of system stability through exhaustive searches of the feedback parameter space. Using this search-based method, we locate a set of maximum feedback parameters based on a phase margin criteria. We then fit continuous equations to this data and obtain a closed-form expression which matches the sampled data to within 2%-4% error for the majority of the parameter space. We apply our feedback parameter selection method to two real-world actuators with widely differing system properties and show that our method successfully produces the maximum achievable non-oscillating impedance response.

1 Introduction

High mechanical output impedance is a common actuation requirement in robotics and related fields. Most robotic positioning systems, such as robotic arms, require high output impedance to minimize positioning error in the presence of unmodeled payloads [1]. Other applications, often in the field of haptics, benefit from actuators capable of exhibiting a wide *range* of impedances [2]. Common to both of these fields are 1) the importance of identifying the upper bound of achievable actuator impedance and 2) their basic control plant model, composed of a force acting on a mass-damper.

The control laws used for haptics and robotic positioning systems share commonalities as well. Haptic devices typically employ impedance control [3] to define a dynamic relationship between external (human) forces acting on the haptic display and the displacement of the haptic display in response to these forces. Robotic positioning systems often rely on the high mechanical output impedance produced by high-gain PID controllers to maintain tracking accuracy in the presence of unmodeled payloads. If we consider cases of PID controllers where the integral term is set to zero, the action of the resulting PD control law depends on the error proportion (P) and its derivative (D). Perhaps the most common impedance model used in haptic displays is that of a virtual spring-damper (K-B) system, which similarly depends on error proportion (K) and its derivative (B). Therefore the analysis of the maximum impedance for a mass-damper plant controlled by a PD-type controller certainly has wide application. Any such analysis should aim to answer two questions: 1) What are the control parameters (i.e. P and D gains) given a set of system parameters (plant properties, feedback delay, etc.) which produce the maximum output impedance? and 2) How is "maximum output impedance" defined? This paper focuses on providing direct and applicable answers to these questions.

Numerous methods exist in literature for selecting feedback control parameters of PID-type systems. Early work utilized knowledge of the system transient response to develop simple equations for determining PID controller values [4]. A number of methods have been developed since, most of which produce PI or PID controller parameters using either numerical or graphical techniques, or by relying on simplifying approximations [5–8]. Effects of nonlinearities due to actuator saturation on selection of PD gains have been studied in [9–11]. More recent approaches apply to a wide range of plants and handle varying levels of controller complexity, including those with filtered D terms, but require inclusion of an integral feedback term [12, 13]. Optimization based methods may also be applied to tune PID controllers for particular performance criteria, but require the use of an optimization framework [14, 15].

It is important to understand what assumptions or criteria apply to the methods used for selecting controller parameters. Perhaps the most conservative criterion is system passivity [16]. Despite its conservative nature, this approach has been widely studied based on the simplicity and elegance of its main result: maximum feedback gains are found using a single closed-form expression. At the other end of the spectrum, several studies are based on a true or false stability criterion, some of which are empirically determined [2, 17–20]. Their observations are useful for system level mechanical design but do not provide the quantitative measures needed for performance-critical controller design. Between these two extremes lie a wealth of methods which produce control parameters given a stability *margin* [7, 8, 12, 21–24]. Other criteria serving a similar purpose include the use of integrated absolute error, maximum sensitivity, Lyapunov-based stability, and others [14, 15, 25, 26].

While prior work provides partial solutions to the problem of determining the maximum control parameters, a complete and readily applicable answer has not been given. As a result, the tuning of the class of systems considered in this paper is often performed using trial-and-error techniques, requiring many hours of tedious work and without any guarantee of finding the optimal parameters. A successful solution to this problem must satisfy a number of requirements. First, it must be simple to apply to enable adoption by a wide audience with varying levels of control systems background, as do the approaches in [4, 8, 16]. Second, it must produce parameters which are not overly conservative, nor parameters which are unstable, so that minimal manual tuning is required, as do the approaches in [7, 8, 12, 14, 15, 21–24]. Third, it must accommodate the full complexity of real-world systems including time delay and filtering of the derivative term, as do the approaches in [2, 12, 14–16, 18, 26]. None of the methods in existing literature meet all three of these requirements.

Is it possible to have a controller tuning method that is simple, meets performance and stability criteria, and captures the full complexity of real-world systems? We show that such a method is indeed possible if we reduce the scope of the problem by 1) considering only a single plant model, 2) considering only critically damped pairs of control parameters, and 3) limiting the range of system parameter values to a finite set. Yet, as previously stated, many systems in practice fit these requirements. The goal of this paper is therefore to provide a simple and effective procedure which applies to a large group of systems (robotic positioning systems and haptic displays, for example) but does not apply to *all* systems. Using these assumptions, we show that it is indeed possible to directly calculate maximum impedance control parameters if system properties are known.

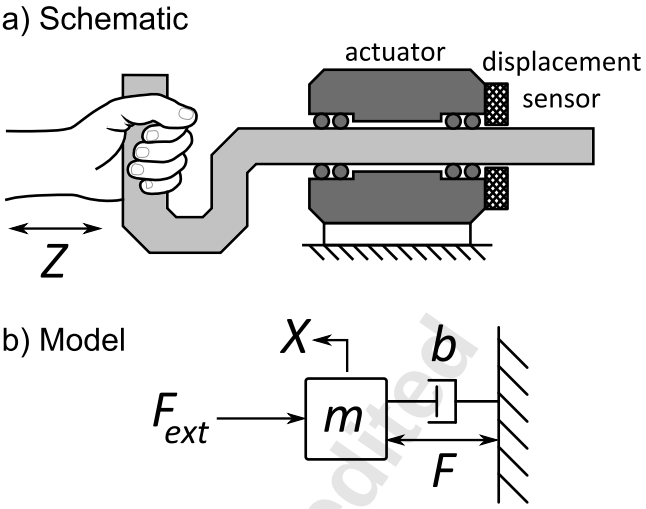

Fig. 1. **a)** An impedance interaction between an actuator and a human. **b)** Model of actuator including forces from external sources.

Our method relies on fitting continuous curves to sets of data derived from simulations of the full control system including time delay and derivative filtering. We use parametric searches to locate critically damped pairs of stiffness and damping parameters meeting a phase margin criteria. As a result, we present a single closed-form equation which accurately maps system parameters to maximum impedance control parameters. Experimental results with a purpose-built actuation testbed demonstrate the efficacy of our method using two different actuators.

2 Problem Statement

Many conventional actuators may be modeled as a force (F) acting on a mass-damper (m-b) (see Figure 1b). The relationship between external forces (F_{ext}) and actuator displacement (X) may be considered to be a form of the output impedance (Z) of the system[1]. External disturbances may be applied by a human as depicted in Figure 1a (originally presented in [2]), or from other sources such as unmodeled actuator loads. The system impedance is a function of both passive system properties ($Z_{passive}$) and impedance caused as a result of forces supplied by the actuator (Z_{active}):

[1] While the mechanical impedance is typically defined as $Z = F/V$ (see [3]), in this work we use the form of mechanical impedance defined by the relationship $Z = F/X$, following the convention used in [27].

$$Z(s) = \frac{F_{ext}(s)}{X(s)} = Z_{passive}(s) + Z_{active} = -ms^2 - bs + Z_{active}. \quad (1)$$

If a feedback control law is defined to produce actuator force as a function of proportional position error (K) and derivative position error (B),

$$F(s) = K(X_d - X) + B(sX_d - sX) \quad (2)$$

then, assuming the desired position (X_d) is set to zero, the system impedance becomes

$$Z(s) = Z_{passive}(s) + Z_{active}(s) = -ms^2 - (b+B)s - K. \quad (3)$$

Notice that the system impedance (3) matches that of a mass-spring-damper system, where the mass is that of the actuator inertia, the damping is the combined passive and active damping, and the stiffness is produced purely via feedback control effort. This "user defined" impedance is the central idea of impedance control [3].

Suppose, as an example, a controller design criteria is given as a maximum tolerable position error (X_{err}) for some steady state disturbance force. In this case, the steady state impedance, $Z(s=0) = K$, can be chosen as:

$$K = \frac{F_{ext}}{X_{err}}. \quad (4)$$

Then, B may be chosen given some desired damping ratio (ζ_d):

$$B = 2\zeta_d\sqrt{mK} - b. \quad (5)$$

For this example, this procedure will work for arbitrarily large values of K and B. However, the same is not true for real-world systems. The impedance model in (3) does not accurately portray the effects of control loop delay and derivative signal filtering which together limit achievable system impedance [2, 26].

If we create a model which includes the effects of control loop delay and derivative signal filtering, we obtain the controller depicted in Figure 2. In this diagram, the actuator model (P) represents the dynamic relation between input motor current (i) and output position (X) given knowledge of the speed reduction (N), motor torque constant (k_τ), and drivetrain efficiency (η):

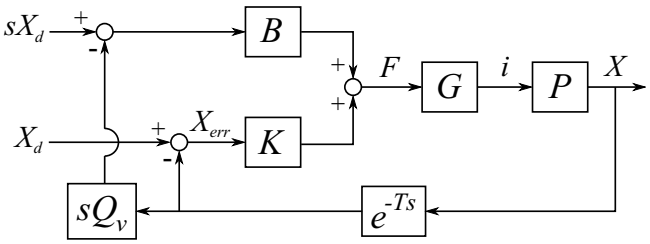

Fig. 2. A spring-damper (K-B) impedance control model with delay (e^{-Ts}) and velocity filtering (Q_v). No force feedback is used, desired forces are simply translated into desired currents.

$$P(s) = \frac{X(s)}{i(s)} = \frac{X(s)}{F(s)}\frac{F(s)}{i(s)} = \frac{Nk_\tau\eta}{ms^2 + bs}. \quad (6)$$

A scaling constant (G) is used to map desired forces into motor currents

$$G = \frac{i(s)}{F(s)} = \frac{1}{Nk_\tau\eta}. \quad (7)$$

To account for the effects of delay and filtering, two additional blocks are added to the control diagram. The e^{-Ts} block represents a time delay of T seconds while the sQ_v block represents the Laplace differentiation operator, s, multiplied by a first-order low-pass filter, Q_v, with a cutoff frequency of f_v Hertz:

$$Q_v(s) = \frac{\omega_v}{s+\omega_v} = \frac{2\pi f_v}{s+2\pi f_v} = \frac{1}{\tau_v s + 1}. \quad (8)$$

The transfer function from desired position, X_d, to measured position, X, for the control system in Figure 2 can be found to be

$$\psi(s) = \frac{X(s)}{X_d(s)} = \frac{Bs+K}{ms^2 + bs + e^{-Ts}(BQ_v s + K)}. \quad (9)$$

As a check, for the case where there is no delay ($T = 0$) and where an unfiltered velocity signal is available ($Q_v = 1$), (9) simplifies to the familiar second-order mass-spring-damper equation.

What are the maximum values of K and B when delay and filtering are not ignored? This is a difficult question to answer for several reasons. First, the function describing maximum K and B values is affected by many system parameters. In the idealized system previously discussed, there was no maximum value of K, and B was a function of four parameters $B = f(\zeta_d, m, b, K)$ where f is the well-known function (5). We would like to find such a closed-form expression for

K_{max} and B_{max} using the non-idealized system model (9). In this case, we must find a function f which maps passive system parameters *and* non-idealized parameters such as delay (T) and filter cutoff frequency (f_v) to a single set of K's and B's:

$$[K_{max}, B_{max}] = f(\zeta_d, m, b, T, f_v). \tag{10}$$

A second complicating factor is that systems with pure delay cannot be analyzed using conventional pole/zero techniques unless approximations of the e^{-Ts} term are used. The delay term makes analysis of the system's behavior more difficult and necessitates the use of alternate stability analysis methods, such as the Nyquist Stability Criterion.

A third difficulty lies in how the word "maximum" is defined. Are the maximum values of K and B the largest values that ensure system passivity, system stability, or some system stability margin?

The following sections discuss how our parameter selection approach addresses these issues.

3 Our Approach

The goals of this section are to address the questions raised in Section 2, namely 1) to identify an appropriate selection criteria for K, and B, and 2) to understand the relationships between maximum controller parameters K, B and the system parameters m, b, T, and f_v.

Our approach to answering these questions centers around analysis of stability margins of the complete system transfer function $\psi(s)$, including derivative filtering and time delay. We rely on parametric sweeps to identify trends and gauge the sensitivity of $\psi(s)$ to each system parameter. We use a phase margin threshold instead of a passivity or stability threshold as a trade-off between system performance and robustness.

With an understanding of how $\psi(s)$ depends on the various system parameters, we perform a thorough search of the system parameter space which is intended to encompass a large portion of actuation systems in use today. Based on the data collected from this experiment, we then fit continuous equations to the experimental data. As a result, we obtain a generic closed-form expression which may be used to select values for K and B which yield the maximum actuator impedance meeting our phase margin criteria.

An important theme in the following discussion is the need to reduce the complexity and coupling between parameters of (10). We simplify the problem by considering a dependent set of K and B values where one may be calculated if the other is known using critically damped assumptions. Using the phase margin thresholding criteria, we observe a useful relationship between maximum closed-loop impedance and the passive system corner frequency which allows us to treat m and b as a single term.

Our approach relies heavily on sampled simulation data and not on theoretical proofs. Therefore, the results shown in this paper should be taken as evidence, not proof, that such relationships exist.

3.1 A Critically Damped Constraint

Let us assume a critically damped impedance response is a design constraint. A critically damped response has several desirable properties such as a near-minimum settling time (assuming a small error-band tolerance) and a high stability margin. In addition, a critically damped constraint reduces the solution space of (10) from a two degree of freedom plane of K's and B's to a single array of critically damped K-B pairs. These K-B pairs can be usefully characterized by their natural frequency, f_n, where

$$\omega_n = 2\pi f_n = \sqrt{\frac{K}{m}} \tag{11}$$

and B is selected using (5) with $\zeta_d = 1$. In the remainder of this paper, it is assumed that when we discuss varying f_n, we do so by altering K (and B to maintain the critically damped constraint), and not by choosing a different m. Therefore, there is a direct correlation between f_n, the values of K and B, and actuator impedance.

It is important to note here that while we place a critical damping constraint on the selection of K and B, this does not guarantee that the dynamic response of the system transfer function ($\psi(s)$) will be critically damped. The reason for this is because (5) only guarantees critical damping for second-order systems and $\psi(s)$ is not a second-order system. Therefore, the main purpose for the critically damped constraint is to reduce the solution space, not to guarantee absence of overshoot or other critically damped properties in the dynamic response of $\psi(s)$. The selection of parameters to guarantee a desired response of $\psi(s)$ is the topic of the remainder of this paper.

Using the critically damped constraint, the solution space of (10) is reduced to a single degree of freedom and is a function of four variables:

$$f_{n_{max}} = f(m, b, T, f_v). \tag{12}$$

Suppose that, for the system described by (9), f_n is varied while m, b, T, and f_v remain constant. If we measure the step response for each of these permutations of $\psi(s)$ we obtain the results shown in Figure 3. As f_n is increased (and thus K and B are increased) the response becomes faster. If f_n is increased too far, the response begins to deviate from the shape of a critically damped response and begins to oscillate. The figure also shows the system's phase margin for each response (obtained using the Matlab `margin` command). The phase margin is a measure of stability, higher being more stable and more damped and lower being less stable and more vibratory. The phase margin is a useful metric in this case because it may be calculated for systems with pure time delay (see [21, 22] for more information).

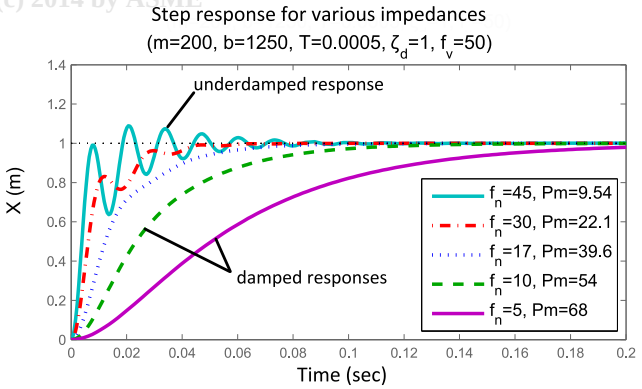

Fig. 3. Step response of $\psi(s)$ for various values of f_n. The phase margin (Pm) of each response is shown. Response deformation begins to occur at a phase margin of 39.6 degrees and large oscillations are visible for a phase margin of 9.54 degrees.

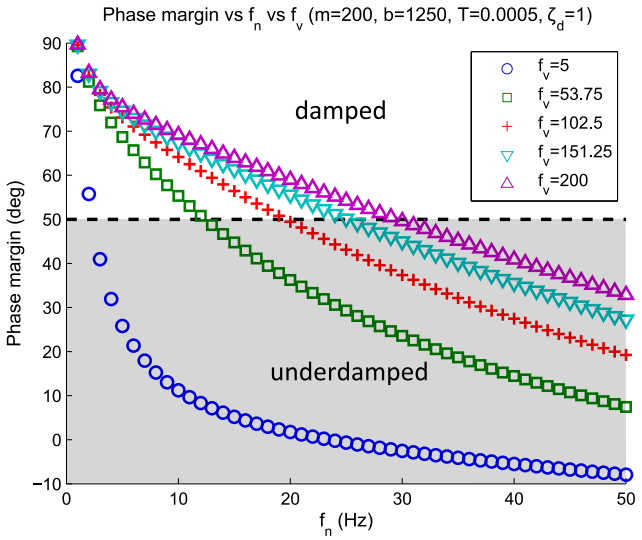

Fig. 4. Phase margin of $\psi(s)$ for various values of f_n and f_v. The system is destabilized either by heavily filtering the derivative term (lower f_v values) or by increasing feedback gains (higher f_n values). A phase margin threshold is shown at 50 degrees. This threshold is determined by observing the minimum phase margin step response which does not exhibit oscillatory distortion in Figure 3. Parameter combinations producing phase margins above this line are represented by an 'o' in Figure 5 while those below are represented by an 'x'.

The oscillation shown in Figure 3 is caused by the combined effects of derivative feedback filtering frequency, f_v, and time delay, T. To gain more insight into this phenomenon, we can perform a similar experiment as before, but this time we vary both f_v and f_n while the other parameters remain constant. If instead of plotting the time domain response, we plot each response's phase margin, we obtain the results shown in Figure 4. Here, we can see how the system phase margin, and thus its dynamic response, is a nonlinear function of f_n and f_v.

These two experiments yield useful insights. First, they demonstrate a relationship, albeit complex, between system

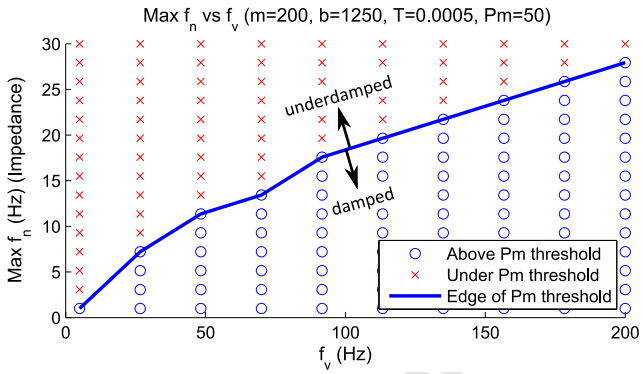

Fig. 5. A parametric search of phase margins of $\psi(s)$ across values of f_n and f_v. Combinations producing phase margins (Pm) above the Pm threshold are represented by an 'o' while those below are represented by an 'x'. The line represents the maximum values of f_n which pass the phase margin criteria and is analogous to the dashed line seen in Figure 4.

stability, feedback gains, and the level of filtering applied to the derivative term. They also demonstrate a connection between the effective damping ratio of the system's step response and the system's phase margin. Clearly, a phase margin of 9.54 degrees produces an underdamped step response for these parameters while phase margins above 54 degrees appear to possess a more damped response.

3.2 A Phase Margin Criteria

Phase margins are known to relate to system damping [21, 22]. Suppose, based on the results shown in Figures 3 and 4, we consider any system with a phase margin greater than 50 degrees to possess a damped, non-vibratory step response. Note that when $\zeta_d = 1$ this characteristic dynamic response is similar to a second-order system's critically damped response in that it has a fast rise time yet does not exhibit periodic signal content. However, the response of $\psi(s)$ cannot be directly compared to a second-order system due to the effects of filtering and delay. The phase margin criteria is independent of the source of instability, whether it is caused by f_v being small, T being large, or some other cause. Regardless of the numerical value of this phase margin threshold, the following analysis may still be performed.

Performing the same search as was used in the experiment for Figure 4, where f_v and f_n are varied while other parameters remain constant, we may instead plot the result of a boolean comparison of each system's phase margin with a phase margin threshold of 50 degrees. Figure 5 shows such a search. For each combination of f_n (y-axis) and f_v (x-axis), an 'o' represents a phase margin greater than 50 degrees while an 'x' represents a phase margin below 50 degrees. The line connecting the maximum values of f_n represents the highest impedance, or the highest values of K and B, which satisfy our phase margin requirement. As before, we see that larger values of f_v produce a more stable system, but now we are able to identify the maximum f_n corresponding to each value of f_v.

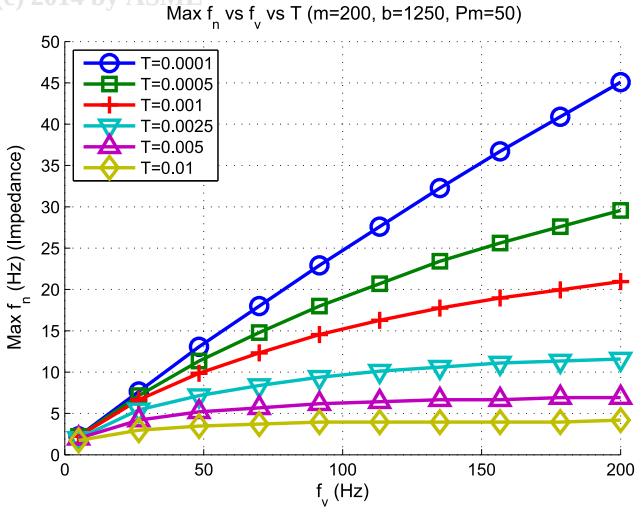

Fig. 6. A parametric search similar to the search in Figure 5 except with higher vertical resolution and an added dimension showing sensitivity to time delay, T. Because f_n represents specific values of K and B, this plot can be used to find the maximum values of K and B, given f_v and T, which produces an impedance controller with a phase margin of 50 degrees.

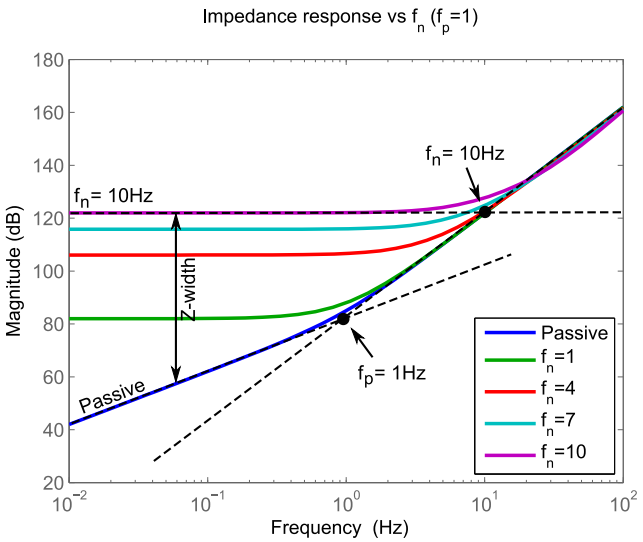

Fig. 7. Impedance frequency response (F_{ext}/X) of an actuator with various closed-loop gains (K,B,$\zeta_d = 1$) determined by f_n. With K and B set to zero, the impedance response is that of the passive actuator. The open loop passive corner frequency (f_p) is shown as well as the closed-loop natural frequency (f_n) for f_n = 10Hz. The difference between maximum and passive impedance, Z-width, is also illustrated.

Going one step further, we can add T as an additional search parameter. Figure 6 shows these results. For clarity, only the boundary lines are shown defining maximum values of f_n. We gain several insights from Figure 6:

1. Achievable impedance increases with f_v (heavily filtering velocity feedback reduces stability).
2. Achievable impedance increases as T decreases (large delay reduces stability).
3. The numerical value of f_v becomes less important as T increases.

The results shown in Figure 6 are enough to fully describe a single system, characterized by its values of m and b. We can easily select K and B values by using Figure 6 as a look-up table to obtain f_n given f_v and T. With f_n found, K and B can be calculated using (11) and (5). However, if we select a different m or b value, the results of Figure 6 will no longer be valid. The next section focuses on the generalization of these results to apply to a wider range of systems.

4 Generalization

The goal of this section is to take the results shown in Figure 6, which only apply to a single pair of m-b values, and generalize them to a wide range of actuators characterized by different m's and b's. Our goal is to find an equation which closely matches a discrete set of data points generated from parametric searches. The data points are the maximum values of f_n ($f_{n_{max}}$) as a function of m, b, T, and f_v which produce phase margins no smaller than 50 degrees. Therefore, a continuous function should be in the form of the function f from (12). Recall from Section 3.1 that f_n is directly related to closed-loop actuator impedance, and therefore maximum system impedance is obtained through $f_{n_{max}}$.

Let us consider the closed-loop impedance transfer function (3). If we plot impedance magnitude versus frequency for various values of f_n we obtain the results shown in Figure 7. If K and B are set to zero, then the impedance of the actuator reduces to the impedance of the passive system. Since the passive impedance is purely a function of velocity and acceleration, the impedance drops to zero as the frequency decreases. That is, the passive system does not respond to constant position offsets; it has no "stiffness." If we select non-zero values of K and B we see how impedance at low frequencies increases, as does the bandwidth of the impedance response.

This frequency representation is useful as it allows us to visualize the closed-loop natural frequency, f_n, as well as the corner frequency of the passive system, f_p. f_p can be found given m and b as follows:

$$\frac{V(s)}{F(s)} = \frac{1}{ms+b} = \frac{1/b}{\tau_p s+1} = \frac{1/b}{\frac{s}{2\pi f_p}+1} \tag{13a}$$

$$f_p = \frac{b}{2\pi m} = \frac{\omega_p}{2\pi}. \tag{13b}$$

We use these relationships in the following section to understand the influence b and m have on $f_{n_{max}}$.

4.1 The Effects of b and m on Maximum Impedance

In earlier work, b has often been solely considered as the system parameter affecting achievable closed-loop impedance [16,18,19,28,29]. A conclusion was drawn, then, that to maximize impedance, a large b is necessary. However, these studies do not directly analyze the influence of m on system impedance.

If we solve (11) for K, substitute K into (5), refactor (9) based on these expressions of K and B with $\zeta_d = 1$, and divide by m, we obtain another representation of $\psi(s)$ which is a function of natural frequency (ω_n), passive corner frequency (ω_p), delay (T), and derivative filter frequency (ω_v):

$$\psi(s) = \frac{(2\omega_n - \omega_p)s + \omega_n^2}{s^2 + \omega_p s + e^{-Ts}[(2\omega_n - \omega_p)Q_v s + \omega_n^2]}. \qquad (14)$$

From (14) it is apparent that the stability of $\psi(s)$ does not change with b as long as ω_p (or the ratio of b/m) is held constant. It is then ω_p (or $f_p \propto b/m$), not b alone, which determines the maximum feedback gains, and thus the maximum impedance of the closed-loop actuation system. Note that this observation does not contest the conclusions drawn in [2,18,19,28,29]. Indeed, if m is held constant then achievable closed-loop impedance increases with b.

The observation of maximum impedance dependency on the ratio of b/m rather than b alone could offer useful insight towards designing devices for high output impedance. For example, device designers attempting to maximize output impedance who were operating based on the recommendations of [16, 18, 19, 28, 29] would attempt to maximize sampling rate (minimizing T) and may either maximize b or make b controllable or tunable. The prior work in this area makes no recommendation on how to select m. It is true that m may vary, for example, based on human grip in haptic devices or based on kinematic configuration in redundant manipulators, but its influence is still important nonetheless. One interesting example of the influence of m on device design could be the selection of actuator speed reduction, N, as it critically influences the magnitude of the actuator load inertia seen by the motor; larger values of N correspond to lower actuator sensitivity to load inertia based on the $1/N^2$ relationship between load inertia and the effective inertia seen by the motor.

Dependency on the ratio b/m greatly simplifies the generalization process. If, for example, $f_{n_{max}}$ were a function of b alone, the units of b would affect the calculation of $f_{n_{max}}$. In SI units, rotary damping is represented by Nms/rad where linear damping is represented by N/m. An equation which accepts units of rotary damping would have to be altered to produce the same results for units of linear damping. Or, the units could be normalized to some predetermined reference frame before being passed to an equation. Dependency on the ratio of b/m removes this issue as both linear and rotary systems may be represented by their respective time constants, τ_p, or corner frequencies, f_p.

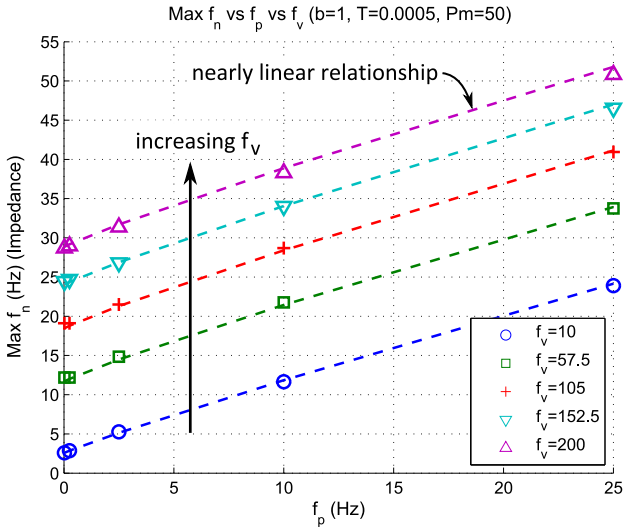

Fig. 8. Parametric search of maximum impedance for various values of f_p and f_v. A relation which is strongly linear can be seen between $f_{n_{max}}$ and f_p. The markers represent simulation data while the dashed lines represent values calculated using (16).

In contrast to (12), dependency on f_p allows us to further simplify the function describing $f_{n_{max}}$:

$$f_{n_{max}} = f(m,b,T,f_v) \Rightarrow f(f_p,T,f_v). \qquad (15)$$

4.2 Fitting Curves to Sampled Data

To study the relationship between f_n, f_p, and f_v further, we perform a search of maximum impedance parameters across values of f_p and f_v (see Figures 8 and 9). The results show a relationship between maximum f_n and f_p which is very nearly linear. f_v then acts as an offset to this linear relationship. This observation creates the basis of our generalization strategy.

Let us assume that there is a relationship between maximum f_n and f_p which is *almost* linear. For some unknown variables c, d, and e, we can represent this relationship with the following equation:

$$f_{n_{max}}(f_p,f_v,T) = c(f_p)^d + e. \qquad (16)$$

The problem of finding a closed-form expression describing maximum f_n is now reduced to a surface fitting problem of c, d, and e which are each a function of f_v and T.

To fit a surface to c, d, and e, we perform a series of searches which cover our desired parameter space. The wider the search space, the more generally applicable a closed-form solution will be. Keeping in mind the scale-independent nature of the f_p parameter, the authors believe a large percentage of actuators in existence today fit within the search space shown in Table 1. The most viscous joints

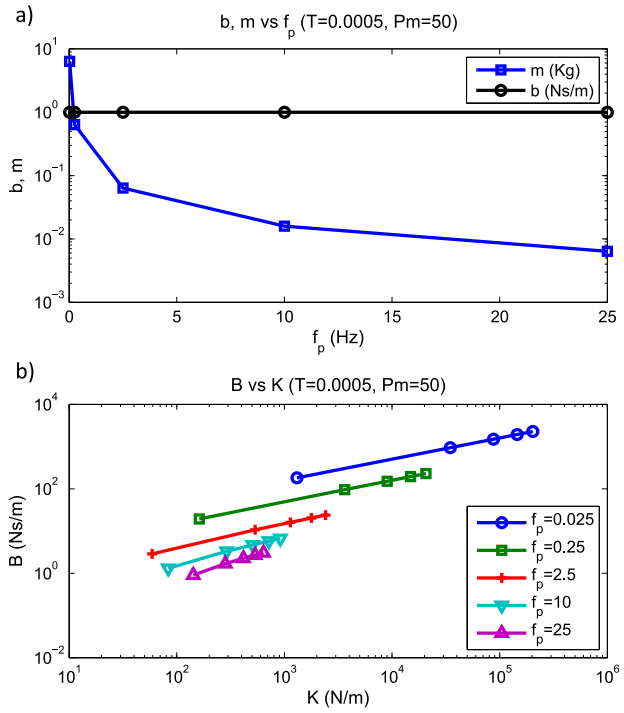

Fig. 9. **a)** Search space of m and b for the experiment shown in Figure 8. **b)** Solution space of K and B for the experiment shown in Figure 8. Each point represents a K-B pair producing a system with the target phase margin.

Table 1. Fitting bounds of $f_{n_{max}}$ equation

Parameter	Search space	Units	Orders of magnitude
f_p	$0.025 \rightarrow 25$	Hz	3
f_v	$10 \rightarrow 200$	Hz	1.3
T	$0.0001 \rightarrow 0.01$	Seconds	2

on NASA-JSC's humanoid Valkyrie robot[2] [30] with grease-lubricated harmonic drive actuators have an f_p value of 9.9 Hz, while the low friction ball screw actuator shown in Section 6 has an f_p value of 0.77 Hz. A standalone 200W electric motor (Maxon EC-powermax 30) only has friction from its bearings and therefore has a lower f_p value of 0.18 Hz. Values for f_v depend primarily on the amount of sensor noise present in the position encoder signal, but based on the author's experience values in the 20-70 Hz range are common. Sampling rates in the range of 1000 Hz (T = 0.0005 seconds) are widely used in robotic servo systems.

After performing a series of searches using automated scripts we were able to find suitable fits for c, d, and e with low error bounds. Polynomial fits produced the best results for the c and d parameters, while a more exotic form based on

[2]The authors spent a year working with the Valkyrie robot during the 2012-2013 portion of the DARPA Robotics Challenge.

Table 2. $f_{n_{max}}$ equation parameters

Index	c	d	e
1	1.093	0.9544	-14.77
2	0.004883	-0.001039	0.4916
3	-54.2	-51.65	2.908
4	-3.694e-5	9.111e-6	-10
5	-0.2871	0.0638	-0.5162
6	1.541e4	6918	0.2257
7	9.201e-8	-2.451e-8	0.2566
8	-4.08e-4	1.559e-4	0.08373
9	49.89	-13.29	0.3725
10	-9.713e5	-3.869e5	n/a

power fitting produced the best results for e. The equations for each of these parameters are as follows:

$$c(f_v,T) = c_1 + c_2 f_v + c_3 T + c_4 {f_v}^2 + c_5 f_v T + c_6 T^2 + c_7 {f_v}^3 + c_8 {f_v}^2 T + c_9 f_v T^2 + c_{10} T^3 \quad (17a)$$

$$d(f_v,T) = d_1 + d_2 f_v + d_3 T + d_4 {f_v}^2 + d_5 f_v T + d_6 T^2 + d_7 {f_v}^3 + d_8 {f_v}^2 T + d_9 f_v T^2 + d_{10} T^3 \quad (17b)$$

$$e(f_v,T) = e_1 T^{e_2} + e_3 + (f_v + e_4)(e_5 {f_v}^{e_6} T^{e_7} + e_8 f_v T + e_9). \quad (17c)$$

The numeric values of the 29 parameters used in equations (17a - 17c) can be found in Table 2.

An example of the surface fit for the d parameter is shown in Figure 10. As can be seen, the continuous surface closely matches the simulation values. The coefficient of determination (R^2) for this fit is 0.986.

The accuracy of this closed-form approximation can be seen for $T = 0.0005$ seconds in Figure 8 where the dashed lines represent the closed-form approximation and the markers represent the real simulation values. Additionally, Figure 11 shows the fitting accuracy of the $f_{n_{max}}$ equation over the entire parameter space, using averaged values for the f_v parameter. As can be seen, for the majority of the parameter space the $f_{n_{max}}$ equation closely fits the ideal simulation values (2-4% error). Peak error of 21% occurs in the corner case when $T = 0.01$ seconds and $f_p = 0.025$ Hz.

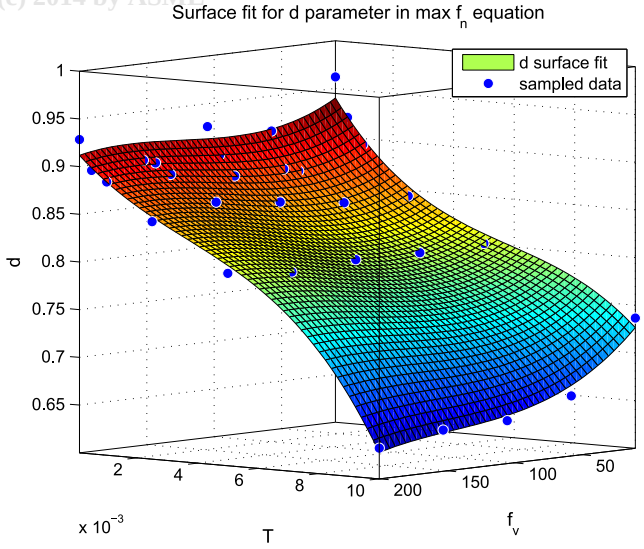

Fig. 10. An example of the fitting process used to match the continuous $f_{n_{max}}$ equation to data points gathered from simulation. This fit represents the d term in (16), (17b).

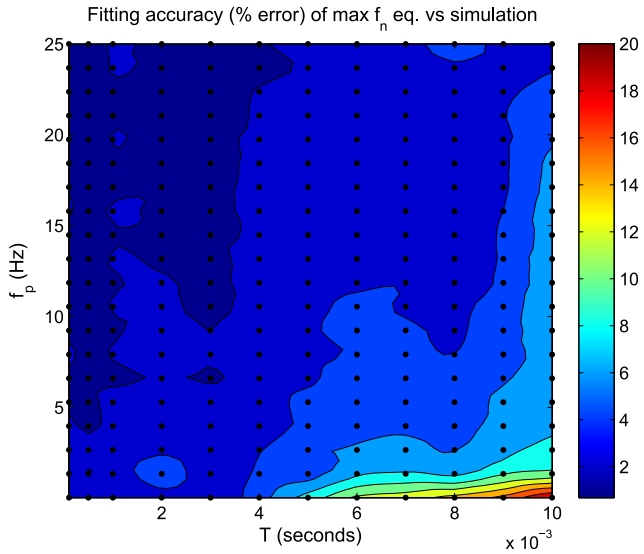

Fig. 11. A graphical representation of the fitting accuracy of the $f_{n_{max}}$ equation compared to ground truth simulation values. The 240 sample points are marked on the contour plot. Error values are averaged along the f_v dimension to simplify data representation. Error percentage remains below 5% for values of T <0.005 seconds. Maximum error (21%) occurs in the corner case where T=0.01 seconds and f_p=0.025 Hz.

4.3 An Example: Applying the $f_{n_{max}}$ Equation

One of the primary benefits of equation (16) is that it transforms gain tuning of rigid actuators with position feedback from a guess-and-check process to a simple and deterministic process. Here we demonstrate how this procedure is applied.

First, m and b must be identified. Section 6.1 provides one method for accomplishing this using a linear actuator of our design.

With m and b known, we can calculate the passive corner frequency, f_p:

$$f_p = \frac{b}{2\pi \cdot m} = \frac{1250}{2\pi \cdot 256} = 0.77\,\text{Hz}. \tag{18}$$

We then need T and f_v to solve for $f_{n_{max}}$. T should be calculated as T = round trip communication latency + sampling period / 2. In our case, we are using a computer directly connected to the actuation hardware and so the effective delay is dominated by the sampling period ($T = 0.0005$ seconds for a sampling rate of 1kHz). f_v can be found by implementing the B term of the impedance controller in hardware for some large but stable value of B and slowly increasing f_v until just before noise is felt or heard when backdriving the output. In our case, we chose $f_v = 50$ Hz. If noise is felt or heard for the final values of K and B, f_v should be reduced and $f_{n_{max}}$ recalculated.

Once f_p, f_v and T have been found, we may then solve for $f_{n_{max}}$ using (16):

$$f_{n_{max}}(f_p = 0.77, f_v = 50, T = 0.0005) = 11.4\,\text{Hz}. \tag{19}$$

K can then be found using (11):

$$\begin{aligned} K_{max} &= (2\pi \cdot f_{n_{max}})^2 \cdot m = (2\pi \cdot 11.4)^2 \cdot 256 \\ &= 1,313,437\,\text{N/m}. \end{aligned} \tag{20}$$

Finally, B is found using (5) with critical damping ($\zeta_d = 1$):

$$\begin{aligned} B_{max} &= 2\zeta_d\sqrt{mK_{max}} - b = 2 \cdot 1\sqrt{256 \cdot 1313437} - 1250 \\ &= 35,423\,\text{N} \cdot \text{s/m}. \end{aligned} \tag{21}$$

We show the experimental results of applying these values in Section 6.

5 Comparisons with Passivity Approach

In [2], equations are provided for determining maximum values for K and B based on a passivity criterion:

$$b > \frac{KT}{2} + \frac{BT}{2\tau_v + T} \qquad (B \geq 0) \tag{22a}$$

$$b > \frac{KT}{2} - B \qquad (B < 0). \tag{22b}$$

If we apply the critically damped constraint from Section 3.1, we can solve (22) for a single pair of values for K and B producing the maximum impedance with passivity properties.

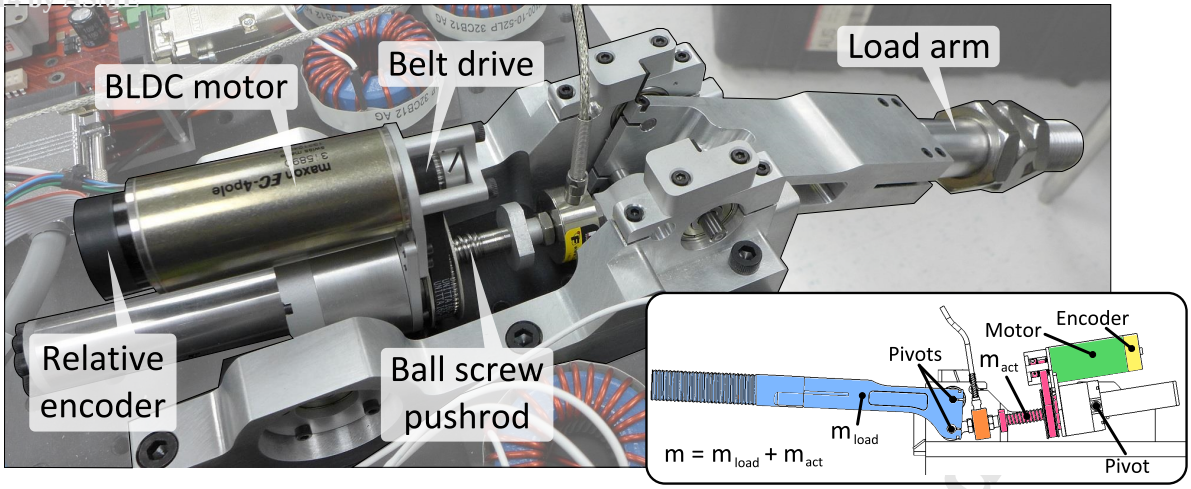

Fig. 13. Ball screw pushrod actuator used in experimental tests. For the standalone motor experiment, the belt was removed so that the motor could spin freely. In the full actuator experiment, the belt was connected, coupling motor motion to ball screw and load arm motion. The depicted load cell is unused in these tests.

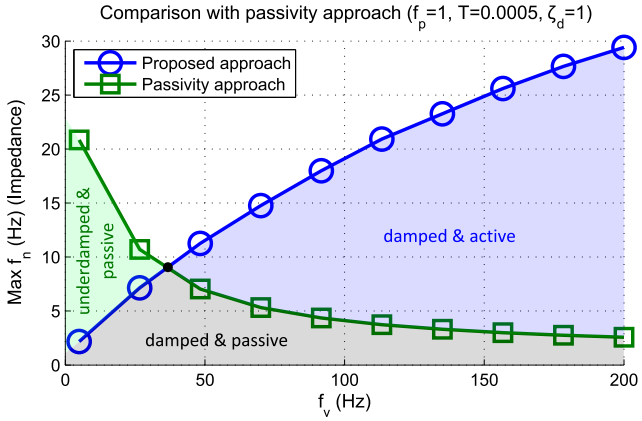

Fig. 12. A comparison between maximum impedance for gains selected by the proposed approach and gains selected by a passivity approach [2].

Figure 12 shows a comparison of maximum impedance as a function of f_v for our proposed approach (16) and for the passivity approach. A few interesting observations are readily apparent. First, impedance is nearly proportional to f_v from a phase margin standpoint and inversely proportional from a passivity standpoint. Second, the values of the passivity line lying above the proposed line (f_v=10→30 Hz) will produce an underdamped response, while the values of the proposed line lying above the passivity line (f_v=50→200 Hz) will produce an active response, meaning the phase response penetrates the ±90 degree boundary [31]. Third, the intersecting point of the two lines is the maximum damped impedance producing a passive response. Previous work suggests an optimal value for f_v exists but does not propose a way to determine such a value [2]. This point of intersection could prove to be a promising candidate.

6 Experimental Validation

In this section we apply our approach of finding maximum impedance parameters to two different actuation systems. Up to this point, all of our analysis has been performed in a simulation environment. The goal of this study is to check how closely matched the responses of real-world actuators are to actuators we have simulated. Our approach is validated if the responses of the real-world actuators become underdamped for the same parameters that cause the simulated actuators to become underdamped.

The properties of the two actuation systems differ significantly in order to demonstrate the wide applicability of our approach. The first system is a standalone brushless direct current (BLDC) motor. Using the system shown in Figure 13, we disconnect the belt from the ball screw drive and test the motor with no load attached. The motor is a small scale rotary actuator with very little passive damping. The second system is the full actuator shown in Figure 13. The output of the ball screw pushrod is connected to the load arm. Small displacements are used to operate the actuator in an approximately linear region of its load inertia. The actuator is a medium scale linear actuator with a large, two-stage speed reduction (209:1 at the arm output). This actuator is a new design that iterates on the actuator presented in [32] and is intended for use in performance studies. It was designed to further reduce weight and size and improve maintainability compared to the previous iteration. The new design uses a modular spring assembly. For the experiments in this paper, a spring was not used in order to match the model shown in Figure 1b.

6.1 System Identification

To apply (16) we must have an accurate model of m and b. While inertial values may be obtained through datasheets and computer-aided design (CAD), it is prudent to ensure the same values are obtained empirically. Damping values are difficult to anticipate and therefore are best measured directly. Here we provide one method for empirically measuring m and b.

Measuring m and b requires measurement of force and displacement, or one of its derivatives. Force measurement

Table 3. Identified system parameters

Parameter	Standalone motor	Full actuator
m	3.0e-6 $[Kg \cdot m^2]$	256 $[Kg]$
b	3.5e-6 $[Nm \cdot s/rad]$	1250 $[N \cdot s/m]$

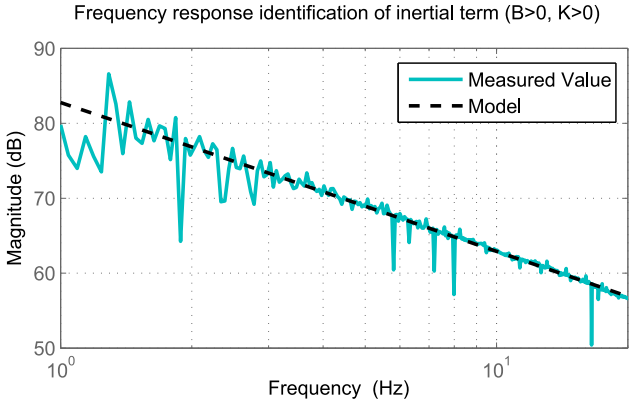

Fig. 14. Experimental identification of inertial (m) model parameter.

may be approximated using current control of electric motors with knowledge of the mapping function between currents and forces (G in (7)), or it may be measured accurately using a load cell.

For systems with variable inertia, control parameters may be selected in several different ways. One option is to select parameters for the scenario where gains are minimized (when m is minimum). This method will produce the most stable system, but will also become underdamped when m is increased. Another option is to select parameters for some nominal value of m. This method will produce a system with trade-offs between control loop stability and performance considered from a damping perspective. A third option is to recalculate stiffness and damping parameters whenever m changes significantly. This method requires higher computational load, but will maintain optimal control parameters throughout the system workspace.

We begin by implementing an arbitrarily stiff impedance controller (that of Figure 2 for example). We then send a chirp signal as a desired position setpoint. By measuring both force and velocity (ensuring the velocity cutoff frequency is greater than the chirp frequency), we can plot the frequency response of these two signals. Then, as shown in Figure 14, an inertia model may be fit to the measured data using the transfer function $\frac{V(s)}{F(s)} = \frac{1}{ms}$.

The b parameter may be measured in a similar way, but depending on the amount of damping and the permissible range of motion, it can be difficult to obtain acceptable data in the lower frequency range. As an alternative we use a closed-loop approach. As before, we implement an impedance controller, but this time we set $B = 0$ and set K to some arbitrarily large value such that it produces an underdamped response. If we send a step in desired position, we

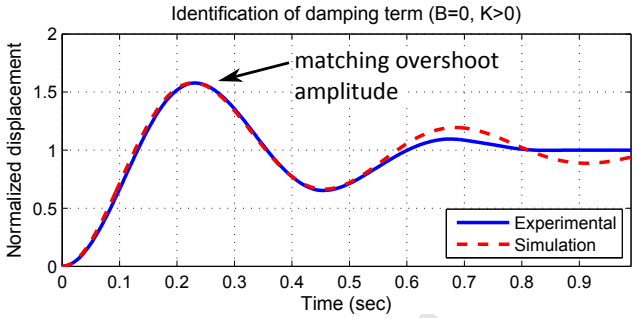

Fig. 15. Experimental identification of damping (b) model parameter using a step response. The deviation seen after 0.5 seconds may be attributed to the presence of unmodeled friction.

may observe the underdamped response and fit this response to a model of the closed-loop system (see Figure 15). The fitting goal should be to produce the same level of overshoot in the model as observed in the experiment.

Using these techniques, we obtained system parameters for the two actuation systems as shown in Table 3. The data for the full actuator is in the linear output reference frame.

6.2 Standalone Motor Experiment

In our first experiment, we observed the dynamic response to a step input of the standalone motor using two sets of impedance control parameters. The first set of parameters was chosen using our proposed approach (16). The second set of parameters was chosen to be greater than the values in the first set, with the hypothesis that higher values should produce an underdamped response (as demonstrated in Figure 3). Specifically, parameters were chosen by doubling the B value obtained from (16), and then selecting K using the critically damped constraint. Figure 16 shows the results. In Figure 16a, we first observe that, for both sets of parameters, the experimental data closely matches the simulation data. Second, it shows that the parameters obtained using the proposed method produce a damped response while the second set of parameters produce a response with small oscillations. This result confirms that, for this case, our proposed method functions as expected and accurately provides the maximum critically damped parameters in practice.

Figure 16b shows the deviation of the experimental results from the simulation results. In the worst case, error reaches just 6% of the full range of the step amplitude indicating that the experimental results closely match the model.

6.3 Full Actuator Experiment

Our second experiment is similar to the motor experiment, except that the full actuator was used. Two sets of impedance parameters were again tested, the first chosen using our proposed approach (16) and the second set chosen to be greater than the values in the first set. Figure 17 shows the results. Here, the results are similar to the motor experiment, except that the deviations between the experimental data and the model are greater. The extra deviation is likely caused by the dynamics of the drivetrain, particularly the belt, which

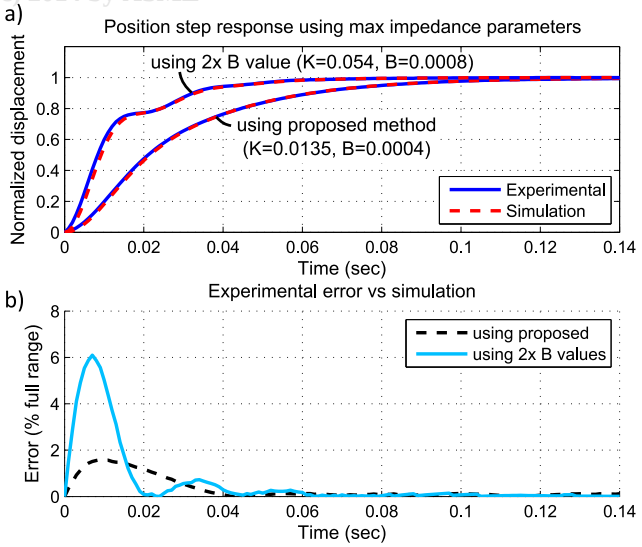

Fig. 16. **Standalone Motor Experiment. a)** Step responses for two different sets of parameters are shown. The first set (proposed method) was obtained using the $f_{n_{max}}$ equation (16). The second set (2x B value) used double the B parameter from the first set, and selected K using the critically damped constraint. The higher gains produce a deformed step response which exhibits small oscillation and therefore exceeds the maximum achievable actuator impedance with a phase margin of 50 degrees. The step displacement for this test was four motor rotations. Due to the high gains used, a higher displacement would cause current saturation to occur (30 amp limit). **b)** Discrepancy between simulation and experimental results. Error peaks at 6% showing the simulation accurately represents real-world effects.

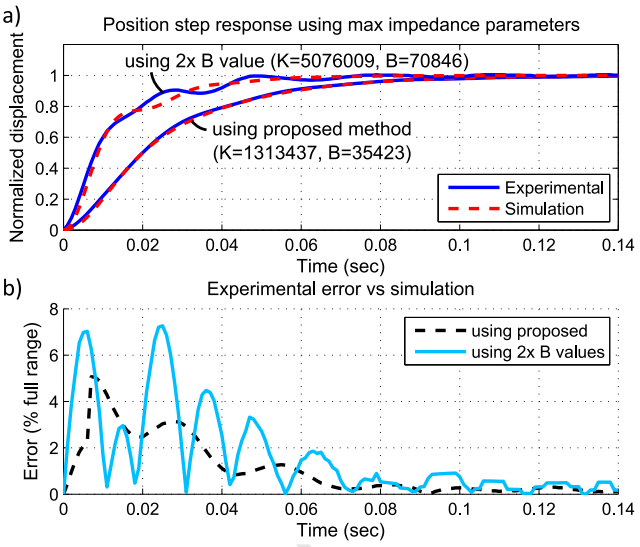

Fig. 17. **Full Actuator Experiment.** The same experiment was performed as was described in Figure 16 except with the full actuator. While the experimental data closely matches simulation data, larger discrepancies can be seen compared to Figure 16. The cause of this increase is likely due to the drivetrain dynamics (particularly the belt). As was the case in the motor experiment, our method again correctly chooses the maximum critically damped control parameters with a phase margin of 50 degrees. The step displacement for this test was 2mm. Due to the high gains used, a higher displacement would cause current saturation to occur (30 amp limit).

may deflect slightly under large torques. Motor current in this test reached values of 15 amps, or more than three times the motor's rated continuous value. Similar deviations may be expected on drivetrains with limited stiffness, such as Harmonic Drives and cable drives. Despite these deviations, error between experiment and simulation remains small, peaking at 7% of full scale.

Perhaps of greater significance than error magnitude is the fact that our hypothesis holds true. Our proposed method produces a response which, upon visual inspection, is well damped, while the higher gains produce a response which is clearly underdamped. These results demonstrate the efficacy of the work presented in this paper. With almost no manual effort and with a single set of equations, we were able to find nearly optimal stiffness and damping feedback parameters for two very different actuations systems.

7 Conclusions

Simple, deterministic procedures have greatly benefited many fields of engineering. In the past, the problem of designing effective high impedance PD-type controllers for rigid actuators has been linked to the problem of designing generic controllers for generic plants. By focusing on a narrower problem, we are able to find a simple and useful method for quickly finding optimal tuning parameters for these systems.

The main outcome of our work is the $f_{n_{max}}$ equation (16) which produces an output value, f_n, given three parameters: control loop delay (T), derivative cutoff frequency (f_v), and a scale-independent representation of the plant parameters (f_p). Knowing f_n is useful because it is directly related to control parameters (gains), which define closed-loop actuator impedance. We derived this complex equation by closely fitting curves to data points obtained through simulation. In the target parameter space, the $f_{n_{max}}$ equation produces values that are generally within 2%-4% of the ideal simulation values.

We have validated the use of the $f_{n_{max}}$ equation on two separate actuators, each of which behaved as modeled in simulation. We believe this equation, and our procedure for applying it, may be greatly beneficial to the robotics and haptics communities, as it quickly provides a set of stiffness and damping gains which produce the maximum damped actuator impedance with a phase margin of 50 degrees.

References

[1] Kawamura, S., Miyazaki, F., and Arimoto, S., 1988. "Is a local linear PD feedback control law effective for trajectory tracking of robot motion?". In Robotics and Automation, Proceedings., IEEE International Conference on, Vol. 3, pp. 1335–1340.

[2] Colgate, J., and Brown, J., 1994. "Factors affecting the Z-Width of a haptic display". In Robotics and Automa-

tion, Proceedings., IEEE International Conference on, Vol. 4, pp. 3205–3210.

[3] Hogan, N., 1985. "Impedance control: An approach to manipulation: Part I-Theory". *Journal of Dynamic Systems, Measurement, and Control,* **107**, pp. 1–7.

[4] Ziegler, J. G., and Nichols, N. B., 1942. "Optimum settings for automatic controllers". *Trans. ASME,* **140**(3), pp. 759–768.

[5] Åström, K. J., 1993. "Automatic tuning and adaptation for PID controllers - A survey". *Control Eng. Practice,* **1**, pp. 699–714.

[6] Lee, C.-H., 2004. "A survey of PID controller design based on gain and phase margins". *International Journal of Computational Cognition,* **2**, pp. 63–100.

[7] Poulin, E., Pomerleau, A., Desbiens, A., and Hodouin, D., 1996. "Development and evaluation of an autotuning and adaptive PID controller". *Automatica,* **32**(1), pp. 71–82.

[8] W. K. Ho, K. W. L., and Xu, W., 1998. "Optimal gain and phase margin tuning for PID controllers". *Automatica,* **34**(8), pp. 1009–1014.

[9] Lawrence, D., 1989. "Actuator limitations on achievable manipulator impedance". In Robotics and Automation, Proceedings., IEEE International Conference on, Vol. 1, pp. 560–565.

[10] Sourlas, D., Choi, J., and Manousiouthakis, V., 1994. "Best achievable control system performance: The saturation paradox". In Decision and Control, Proceedings of the 33rd IEEE Conference on, Vol. 4, pp. 3816–3818.

[11] Goldfarb, M., and Sirithanapipat, T., 1999. "The effect of actuator saturation on the performance of PD-controlled servo systems". *Mechatronics,* **9**, pp. 497–511.

[12] Yaniv, O., and Nagurka, M., 2004. "Design of PID controllers satisfying gain margin and sensitivity constraints on a set of plants". *Automatica,* **40**(1), pp. 111–116.

[13] Åström, K. J., Panagopoulos, H., and Hägglund, T., 1998. "Design of PI controllers based on non-convex optimization". *Automatica,* **34**(5), May, pp. 585–601.

[14] Li, D., Gao, F., Xue, Y., and Lu, C., 2007. "Optimization of decentralized PI/PID controllers based on genetic algorithm". *Asian Journal of Control,* **9**(3), pp. 306–316.

[15] Wang, C., and Li, D., 2011. "Decentralized PID controllers based on probabilistic robustness". *Journal of Dynamic Systems, Measurement, and Control,* **133**(6), Nov, p. 061015.

[16] Colgate, J., and Schenkel, G., 1994. "Passivity of a class of sampled-data systems: Application to haptic interfaces". In American Control Conference, Vol. 3, pp. 3236–3240.

[17] Lawrence, D., 1988. "Impedance control stability properties in common implementations". In Robotics and Automation, Proceedings., IEEE International Conference on, Vol. 2, pp. 1185–1190.

[18] An, J., and Kwon, D.-S., 2004. "In haptics, the influence of the controllable physical damping on stability and performance". In Intelligent Robots and Systems, Proceedings. IEEE/RSJ International Conference on, Vol. 2, pp. 1204–1209.

[19] Mehling, J., Colgate, J., and Peshkin, M., 2005. "Increasing the impedance range of a haptic display by adding electrical damping". In Eurohaptics Conference, Symposium on Haptic Interfaces for Virtual Environment and Teleoperator Systems, pp. 257–262.

[20] Hulin, T., Preusche, C., and Hirzinger, G., 2006. "Stability boundary for haptic rendering: Influence of physical damping". In Intelligent Robots and Systems, IEEE/RSJ International Conference on, pp. 1570–1575.

[21] Franklin, G. F., Powell, J. D., and Baeini, A. E., 1986. *Feedback Control of Dynamic Systems*. Addison-Wesley, Reading, MA.

[22] Ogata, K., 1990. *Modern Control Engineering*. Prentice-Hall, Englewood Cliffs, NJ.

[23] Suchomski, P., 2001. "Robust PI and PID controller design in delta domain". *Control Theory and Applications, IEE Proceedings -,* **148**(5), Sep, pp. 350–354.

[24] Li, K., 2013. "PID tuning for optimal closed-loop performance with specified gain and phase margins". *Control Systems Technology, IEEE Transactions on,* **21**(3), May, pp. 1024–1030.

[25] Lee, C.-H., and Teng, C.-C., 2003. "Calculation of PID controller parameters by using a fuzzy neural network". *ISA Transactions,* **42**, pp. 391–400.

[26] Diolaiti, N., Niemeyer, G., Barbagli, F., and Salisbury, J., 2006. "Stability of haptic rendering: Discretization, quantization, time delay, and coulomb effects". *Robotics, IEEE Transactions on,* **22**(2), April, pp. 256–268.

[27] Pratt, G., and Williamson, M., 1995. "Series elastic actuators". In Intelligent Robots and Systems 95. 'Human Robot Interaction and Cooperative Robots', Proceedings. 1995 IEEE/RSJ International Conference on, Vol. 1, pp. 399 –406 vol.1.

[28] Weir, D., Colgate, J., and Peshkin, M., 2008. "Measuring and increasing z-width with active electrical damping". In Haptic interfaces for virtual environment and teleoperator systems, Symposium on, pp. 169–175.

[29] Rossa, C., Lozada, J., and Micaelli, A., 2013. "Stable haptic interaction using passive and active actuators". In Robotics and Automation, IEEE International Conference on, pp. 2386–2392.

[30] NASA-JSC DRC team valkyrie. http://www.theroboticschallenge.org/node/59. Accessed: 2014-02-10.

[31] Bao, J., and Lee, P. L., 2007. *Process Control: The Passive Systems Approach*. Springer.

[32] Paine, N., Oh, S., and Sentis, L., 2014. "Design and control considerations for high-performance series elastic actuators". *Mechatronics, IEEE/ASME Transactions on,* **19**(3), June, pp. 1080–1091.